Progress In Electromagnetics Research M, Vol. 120, 69–82, 2023

Multi-Objective Optimal Design of Single-Phase Line-Starting Permanent Magnet Synchronous Motor Based on Response Surface Method

Shixiong Yin* **and Aiyuan Wang**

Abstract—Single-phase asynchronous motors have an irreplaceable role in small production fields such as household appliances and office equipment. However, due to the existence of small single-phase asynchronous motors with low power factor, low efficiency, vibration and noise, and other problems, the performance of a single-phase asynchronous motor, including efficiency, power factor, and vibration noise has been unable to meet the increasing needs of people. In this paper, a single-phase line-starting permanent magnet synchronous motor (SPLSPMSM) for air compressor is designed with the core size of Y series three-phase asynchronous motor for reference. The operating capacitance, the number of turns of the main stator winding, the turns ratio of the main and auxiliary windings, and the permanent magnet size are selected as optimization variables, and the efficiency, power factor, and starting torque are the optimization objectives. A regression model was developed by the response surface method (RSM) to optimize the performance of the motor, and the reliability of the response surface experiment was verified. The results show that the performance of the optimized motor is improved in terms of rated operation and starting performance.

1. INTRODUCTION

In low power applications, such as home appliances and small mechanical equipment, single-phase asynchronous motors have an irreplaceable role. Compared to single-phase asynchronous motors, SPLSPMSMs have more obvious advantages in several aspects. At the same output power, SPLSPMSM is usually smaller than single-phase asynchronous motor, and due to its high efficiency, it can effectively reduce energy waste. This is in line with the development strategy of energy saving and environmental protection, and helps to reduce energy consumption and demand for fossil fuels.

In recent years, due to the increasing energy efficiency standards in countries around the world, there are correspondingly higher requirements for the performance design of electric motors. In [1–5], various aspects of the electromagnetic design of line-starting permanent magnet synchronous motors have been optimized to provide a reference for the design of similar motors. Ref. [6] studied and analyzed the starting performance of line-starting permanent magnet synchronous motors to improve the starting performance of single-phase asynchronous motors. Refs. [7–10] improved the performance of the motor by structural adjustment of the motor. Refs. [11, 12] studied the optimization of the performance of such motors drawn into synchronization. Other aspects have also been studied in recent years, such as fault diagnosis [13–15], temperature rise analysis [16, 17], and harmonic suppression [18–20].

Based on the above study, an SPLSPMSM for an air compressor is initially designed with a three-phase asynchronous motor as a reference. Compared with the original single-phase asynchronous motor,

Received 7 July 2023, Accepted 16 October 2023, Scheduled 25 October 2023
* Corresponding author: Shixiong Yin (530738718@qq.com).
The authors are with the School of Electrical Engineering, Shanghai Dianji University, Shanghai, China.

the operating performance of this motor is greatly improved, and some parameters of the motor are optimized by the RSM, which has higher accuracy and better optimization effect than Taguchi method.

This paper is roughly composed of four chapters. Section 2 analyzes the mathematical model of SPLSPMSM in rated operation by means of dual rotating magnetic field theory and symmetric component method, and Section 3 introduces the RSM and the whole process of response surface experiment, and verifies the reliability of the experiment. Finally, the research results of this paper are summarized.

2. PRINCIPLE AND PARAMETERS OF SPLSPMSM

Structurally, SPLSPMSM is similar to a single-phase asynchronous motor, except that SPLSPMSM has permanent magnets added to the rotor to provide the main magnetic field, and permanent magnets can improve the motor's operating performance [21].

In the rated operation phase of SPLSPMSM, the analysis method of single-phase asynchronous motor can be referred to. The phase current and phase voltage of two phases are decomposed by positive and negative sequences using dual rotating magnetic field theory and symmetrical component method. The positive sequence component is calculated by substituting the two-phase PM synchronous motor, and the negative sequence component is calculated by substituting the two-phase asynchronous motor.

$$\begin{aligned} \dot{I}_{m+} &= \frac{1}{2}\left(\dot{I}_m - j\dot{I}_a^{'}\right) = \frac{1}{2}\left(\dot{I}_m - jb\dot{I}_a\right) \\ \dot{I}_{m-} &= \frac{1}{2}\left(\dot{I}_m + j\dot{I}_a^{'}\right) = \frac{1}{2}\left(\dot{I}_m + jb\dot{I}_a^{'}\right) \end{aligned} \tag{1}$$

$$\begin{aligned} \dot{I}_{a+}^{'} &= j\dot{I}_{m+} \\ \dot{I}_{a-}^{'} &= -j\dot{I}_{m-} \end{aligned} \tag{2}$$

where b is the effective turns ratio of the auxiliary winding and the main winding; $\dot{I}_m$ and $\dot{I}_a$ are the main and auxiliary phase currents, respectively; $\dot{I}_{m+}$ and $\dot{I}_{m-}$ are the positive and negative sequence components of the main phase current, respectively; $\dot{I}_{a+}^{'}$ and $\dot{I}_{a-}^{'}$ are the positive and negative sequence components of the converted secondary phase current, respectively. According to the dual-response theory, the vector diagram can be established as shown in Figure 1.

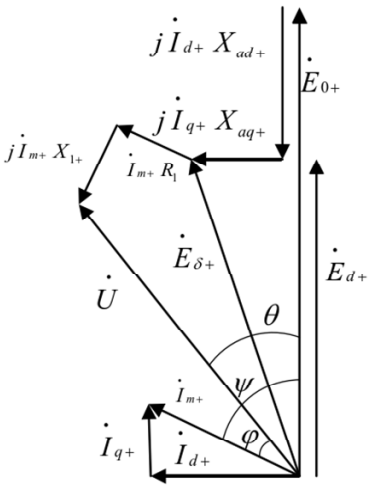

Figure 1. Vector diagram.

The equations for voltage, input power, and electromagnetic torque are as follows:

$$\dot{U}_+ = \dot{E}_{0+} + \dot{I}_m \cdot R + j\dot{I}_{d+} \cdot X_{d+} + j\dot{I}_q \cdot X_{q+} \tag{3}$$

$$P_{1+} = \frac{m\dot{U}_+ \cdot \left[E_{0+}\left(X_{q+} \cdot \sin\theta - R \cdot \cos\theta\right) + R \cdot \dot{U}_+ + 0.5\dot{U}_+ \cdot \left(X_{d+} - X_{q+}\right)\sin 2\theta\right]}{R^2 + X_{d+} \cdot X_{q+}} \tag{4}$$

$$T_{e+} = \frac{P_{1+}}{\omega_+} = \frac{m_+ \cdot p \cdot E_{0+} \cdot U_+}{\omega_+ \cdot X_{d+}} \cdot \sin\theta + \frac{m_+ \cdot p \cdot U_+^2}{2\omega_+} \cdot \left(\frac{1}{X_{q+}} - \frac{1}{X_{d+}}\right) \cdot \sin 2\theta \tag{5}$$

where $\dot{U}_+$ is the positive sequence component of the phase voltage; $\dot{E}_{0+}$ is the positive sequence PMSM no-load counter potential; R is the positive sequence PMSM armature phase resistance; $\dot{I}_{d+}$ is the positive sequence PMSM armature current straight-axis component; $\dot{I}_{q+}$ is the positive sequence PMSM armature current cross-axis component; X_{d+} is the positive sequence PMSM straight-axis reactance; X_{q+} is the positive sequence PMSM cross-axis reactance; m is the number of phases of the PMSM, which is 2 at this time; θ is the PMSM torque angle; p is the number of PMSM poles; ω_+ is the PMSM electrical angular velocity.

The negative sequence current can be calculated by referring to the formula of the three-phase asynchronous motor. The final SPLSPMSM voltage, current, and electromagnetic torque can be synthesized by the vector method, and the final equation is shown below:

$$\dot{I}_m = \dot{I}_{m+} + \dot{I}_{m-}, \ \ \dot{I}_a = \dot{I}_{a+} + \dot{I}_{a-} \tag{6}$$

$$\dot{U}_m = \dot{U}_{m+} + \dot{U}_{m-}, \ \ \dot{U}_a = \dot{U}_{a+} + \dot{U}_{a-} \tag{7}$$

$$T_m = T_{m+} + T_{m-} \tag{8}$$

Referring to the stator-rotor core size of YE3-90 series three-phase asynchronous motor to determine the design parameters of the motor and the current IE energy efficiency standards, the main dimensions and design requirements of the motor are shown in Table 1.

Table 1. Main design parameters of motor.

Parameter name	Value	Parameter name	Value
Stator outer diameter/mm	138	Rated voltage/V	220
Stator inner diameter/mm	85	Rated power/W	1500
Core length/mm	130	Frequency/Hz	50
Rotor outer diameter/mm	84.5	Number of poles	4
Rotor inner diameter/mm	30	Number of stator/rotor slots	32/24
Number of turns of main winding	28	Winding turns ratio	1.55
Width of permanent magnet/mm	30	Thickness of permanent magnet/mm	4
Power Factor	> 0.9	Efficiency/%	> 82.8

The selection of capacitors is very important for SPLSPMSM, which will directly affect the motor's operating performance and starting performance. To select a suitable capacitor, it is necessary to consider the rated power of the motor, the requirements of the starting load, and the requirements of the running performance. Considering the scenario used and the actual capacitor specifications, a 30 μF capacitor is initially selected as the running capacitor and a 200 μF capacitor as the starting capacitor.

The winding of SPLSPMSM can be used in two ways: sinusoidal winding and stacked winding. The sinusoidal winding uses concentric winding, which arranges the turns in each slot according to the fundamental cosine law, thus reducing the harmonic content of the air gap magnetic potential, which can reduce the losses, vibration, and noise during motor operation. However, due to a different number of turns in each coil, this winding manufacturing process is complicated. Double-layer windings must be used, and phase-to-phase insulation is required, leading to a reduction in the effective utilization of the slots. In contrast, stacked windings allow each coil to have the same number of turns, thereby increasing the utilization of the slot and simplifying the manufacturing process. Therefore, if you choose to use stacked windings, you can use a single layer winding without the need for phase-to-phase insulation, thus increasing the effective utilization of the slot and the manufacturing efficiency.

Since the design case of this paper is a motor used in air compressor, the motor structure is relatively small, and the sinusoidal winding structure is relatively complex. Therefore after the initial electromagnetic design comparison, the single-layer stacked winding type is used. The final quarter cross section of the motor is shown in Figure 2.

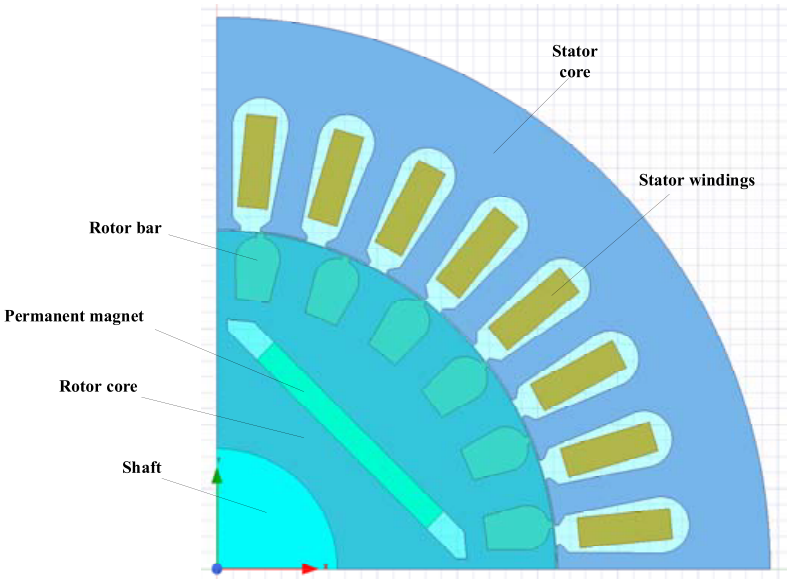

Figure 2. Quarter cross section of the motor.

3. MULTI-OBJECTIVE ANALYSIS OPTIMIZATION BASED ON RESPONSE SURFACE METHODOLOGY (RSM)

3.1. Response Surface Experimental Design

The optimal design of a motor is a very complex process, with many parameters constraining each other. For example, the adjustment of the operating capacitance can improve the efficiency of the motor, but it may lead to a decrease in power factor and starting torque. In the analysis of multifactor quantitative processing data, the regression relationship between the dependent variable and multiple independent variables can be analyzed, and this regression relationship may be curved or curved surface relationship, so it is called response surface analysis. Compared with orthogonal experimental analysis, response surface experimental analysis needs to take more samples, and the results analyzed are more accurate. The regression model between multiple dependent variables and multiple independent variables can be derived. The whole experimental design process is shown in Figure 3.

The SPLSPMSM for air compressors, due to its working environment, gives priority to the efficiency η and power factor PF of this motor as optimization objectives, and secondly, although the starting torque requirements of these motors are not high, they must meet the technical operating conditions of the same speed class and power class motors. Therefore, the starting torque Tst is used as the second optimization target.

After the preliminary electromagnetic calculation analysis, it is concluded that the running capacitance has a greater influence on the rated operation performance and starting performance of SPLSPMSM, so the running capacitance C_r is taken as the first optimization variable; generally for motors with permanent magnets, the size of the permanent magnets will not only affect the rated operation performance of the motor, but also affect the starting performance of the motor at the same time because the permanent magnets will produce braking torque in the starting phase. Therefore, the length W_m and thickness T_m of the permanent magnet are used as the second and third optimization variables; the number of turns in the main winding of the stator affects the generation of the motor's

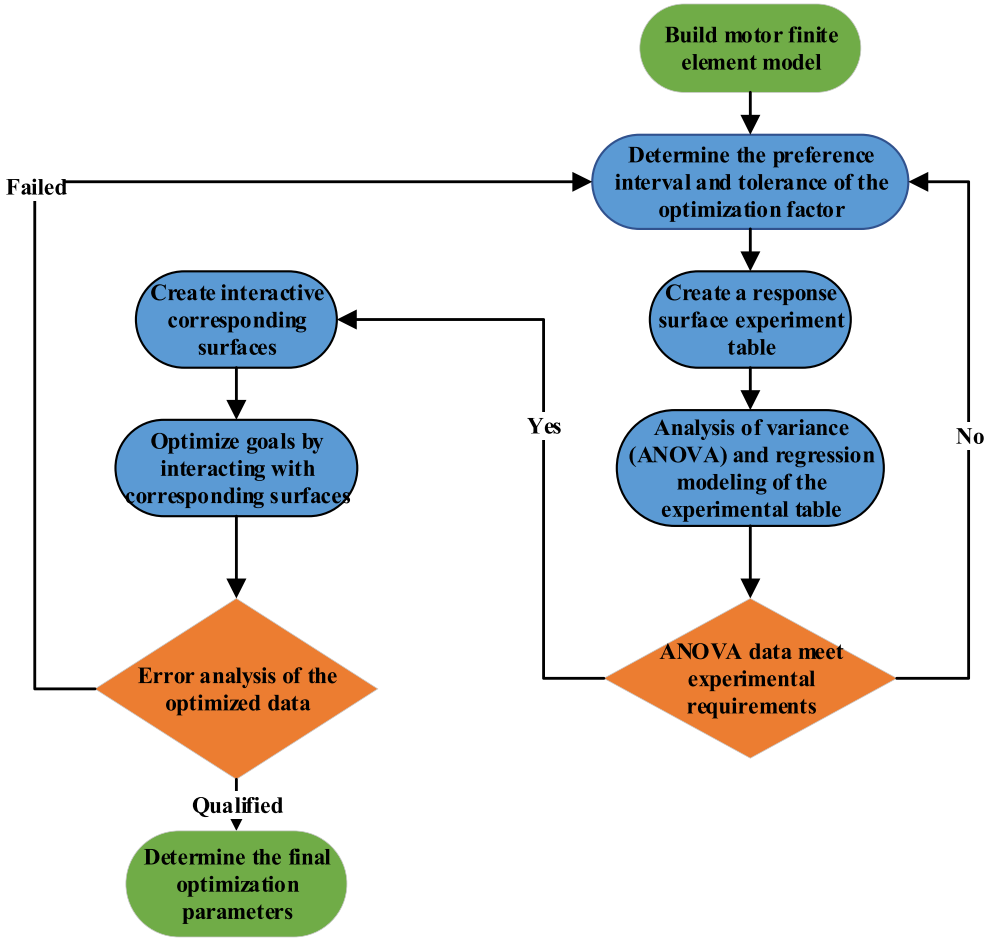

Figure 3. Experimental design flow.

main magnetic field, while the main and secondary winding turns ratios affect the distribution of the secondary magnetic field on the stator. A proper turns ratio can change the distribution of the magnetic field and thus have an effect on torque generation. By choosing the number of turns of the main winding and the ratio of turns of the main and secondary windings appropriately, the torque generating capacity of the motor can be optimized, and the torque can be increased. Therefore, the main winding Na and the main and secondary winding turns ratio R_{ab} are taken as the fourth and fifth optimization variables.

The equations for the optimization variables and performance metrics are as follows:

$$\begin{cases} \mathbf{x} = [x_1, x_2, x_3, x_4, x_5]^T = [C_r, N_a, R_{ab}, T_m, W_m]^T \\ y_i = f_i(\mathbf{x}) \end{cases} \tag{9}$$

The five optimization variables are referred to as A, B, C, D, and E influence factors. After preliminary calculation and comparison of the motor parameters, the five design optimization variables are 30 μF, 30, 1.45, 30 mm, and 4 mm. The values of these variables are used as approximate centers and are extended appropriately in all directions to obtain the range of variation of the design variables. Three levels are set for each design variable. The level grades are selected differently considering the actual dimensions and manufacturing tolerances of the motor design variables. The level grades are 5 μF, 5 and 0.3, 1 mm, and 2 mm, respectively. The influence factors and level grades are shown in Table 2.

The response surface experiment table is established by the 3 Level classes and the influence variables in the above table, where the data in Table 3 have finite element calculations. Due to the large amount of data in the table, only a part of the data in the table are given in this paper, and the specific data are shown in Appendix A. y_1, y_2, y_3 are efficiency, power factor, and starting torque (N·m),

Table 2. Optimization variables and level classes.

Optimization variables \ Level classes		−1	0	1
A	C_r/μF	25	30	35
B	Na	25	30	35
C	R_{ab}	1.1	1.4	1.7
D	T_m/mm	3	4	5
E	W_m/mm	27	29	31

Table 3. Response surface experimental results.

number	A	B	C	D	E	y_1	y_2	y_3
1	30	35	1.7	4	29	79.795	97.003	10.7
2	30	35	1.4	5	29	85.118	97.79	16.597
3	35	30	1.1	4	29	83.99	95.65	16.183
4	30	30	1.7	3	29	80.953	95.291	14.293
5	30	30	1.4	4	29	84.151	95.409	18.085
6	30	30	1.7	4	31	83.671	97.831	16.544
7	30	25	1.1	4	29	72.218	80.444	15.144
8	35	30	1.4	5	29	83.157	96.278	19.39
9	35	30	1.4	4	27	82.059	94.09	17.888
10	35	25	1.4	4	29	73.288	82.569	18.232
11	25	35	1.4	4	29	87.108	97.952	15.718
12	30	30	1.7	4	27	81.627	94.228	15.906
13	30	30	1.1	3	29	83.574	91.589	13.861
14	30	25	1.4	3	29	69.934	72.819	16.058
15	30	30	1.1	5	29	83.094	95.287	17.392
16	25	30	1.4	4	27	83.494	90.679	17.881
17	30	30	1.4	5	27	82.762	93.26	19.643
18	30	30	1.4	5	31	83.779	97.592	19.043

respectively. For the convenience of calculation, the power factor is subsequently calculated to increase 100 times.

3.2. Experimental Procedure

Based on the experimental data in Table 3, the analysis of variance (ANOVA) was performed using the software. And the quadratic polynomial regression model with three optimization objectives of y_1, y_2, y_3 was established.

$$\begin{aligned} y_1 = {} & 84.15 - 0.71A + 5.87B - 0.88C + 0.53D + 1.08E - 1.18AB - 0.62AC + 0.49AD \\ & +0.17AE - 2.29BC - 0.69BD - 0.96BE + 0.62CD + 0.093CE - 0.7DE - 0.12A^2 - 5.11B^2 \\ & -0.64C^2 - 0.9D^2 - 0.31E^2 \end{aligned} \tag{10}$$

$$y_2 = 95.41 + 1.03A + 8.62B + 0.78C + 1.63D + 2.41E - 0.87AB - 0.065AC - 0.63AD - 0.61AE - 0.87BC - 3.74BD - 2.41BE - 0.67CD - 0.54CE - 0.63DE - 0.21A^2 - 5.73B^2 + 0.023C^2 - 0.78D^2 - 0.47E^2 \quad (11)$$

$$y_3 = 18.08 - (9.813E - 003)A - 1.44B - (2.688E - 003)C + 1.64D + 0.097E - 0.053AB - 0.084AC - (6.000E - 003)AD + 0.032AE - 2.27BC - 0.26BD + 0.14BE - 0.1CD + 0.15CE - 0.28DE - 0.021A^2 - 1.1B^2 + 1.91C^2 - 0.36D^2 - 0.069E^2 \quad (12)$$

Tables 4, 5, and 6 show the ANOVA results for the three optimization objectives of efficiency, power factor, and starting torque, respectively. The smaller the P-value is, the more effective the regression model is available, and the greater the influence of the factor is on the optimization objective. From the three tables, it can be seen that all three regression models are highly significant; the coefficient of variation and precision of the three regression models can be obtained from the ANOVA results, and the models are available when the coefficient of variation is less than 10%, and the precision is more than 4. The coefficients of variation of the three regression models are 0.81%, 1.13%, and 2.01%, respectively; the precision is 34.24, 30.6, and 34.91, respectively. The normal probability distribution of the residuals of the three models can be obtained through the software analysis as shown in Figure 4, which shows that the residuals are uniformly distributed around a straight line, which indicates that the regression models are better adapted. From the above analysis, it can be concluded that the three regression models are valid and have very high reliability.

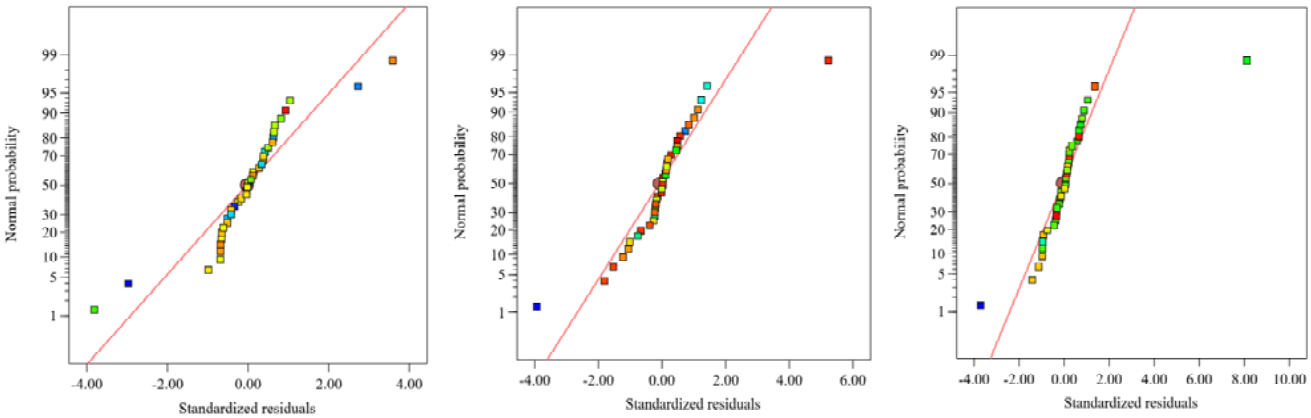

Figure 4. Residual normal probability distribution chart. (a) y_1, (b) y_2, (c) y_3.

3.3. Analysis of Experimental Results

From Table 4, it can be seen that the most influential variables on the efficiency are Na, R_{ab}, and W_m, followed by C_r and T_m. The quadratic polynomial regression model can be used to derive the corresponding surface plot of the interaction effect of Na, R_{ab}, and W_m as variables as shown in Figure 5. From Figure 5, it can be seen that as the number of turns of the main winding Na and the length of the permanent magnet W_m and the ratio of turns of the main and auxiliary windings R_{ab} increase, the efficiency shows a trend of first increasing and then decreasing. Finally, the maximum efficiency is achieved when Na is about 32, R_{ab} about 1.2, and W_m about 30.

As can be seen from Table 5, the shadow of the greatest effect on power factor is Na, W_m, T_m, followed by C_r and R_{ab}. Therefore, the quadratic polynomial regression model can be derived from Na, W_m, T_m as the corresponding surface plot of the interaction effect of variables as shown in Figure 6. From Figure 6, it can be seen that when Na is smaller, T_m is larger for power factor, but when Na increases, T_m is smaller for power factor increase. And the increase of W_m will always increase the power factor. Finally when Na is about 34, W_m is about 31, T_m about 3.1, and the power factor achieves the maximum value.

Table 4. Variance analysis of motor efficiency.

Sourse	Squares	df	Square	P
y_1	832.58	20	41.63	< 0.0001**
A	7.13	1	7.13	0.0008*
B	489.47	1	489.47	< 0.0001**
C	12.4	1	12.4	< 0.0001**
D	4.06	1	4.06	0.0069*
E	16.66	1	16.66	< 0.0001**
AB	5.56	1	5.56	0.0022*
AC	1.55	1	1.55	0.0758
AD	0.94	1	0.94	0.1594
AE	0.073	1	0.073	0.6883
BC	20.92	1	20.92	< 0.0001**
BD	1.26	1	1.26	0.1072
BE	3.65	1	3.65	0.0098*
CD	1.53	1	1.53	0.0781
CE	0.034	1	0.034	0.7828
DE	1.94	1	1.94	0.0493*
A^2	0.043	1	0.043	0.7565
B^2	78.51	1	78.51	< 0.0001**
C^2	1.27	1	1.27	0.1056
D^2	2.44	1	2.44	0.0295
E^2	0.29	1	0.29	0.4248
Residual	7.87	18	0.44	
Total	840.45	38		

"**" indicates that the item is highly significant; "*" indicates that the item is significant

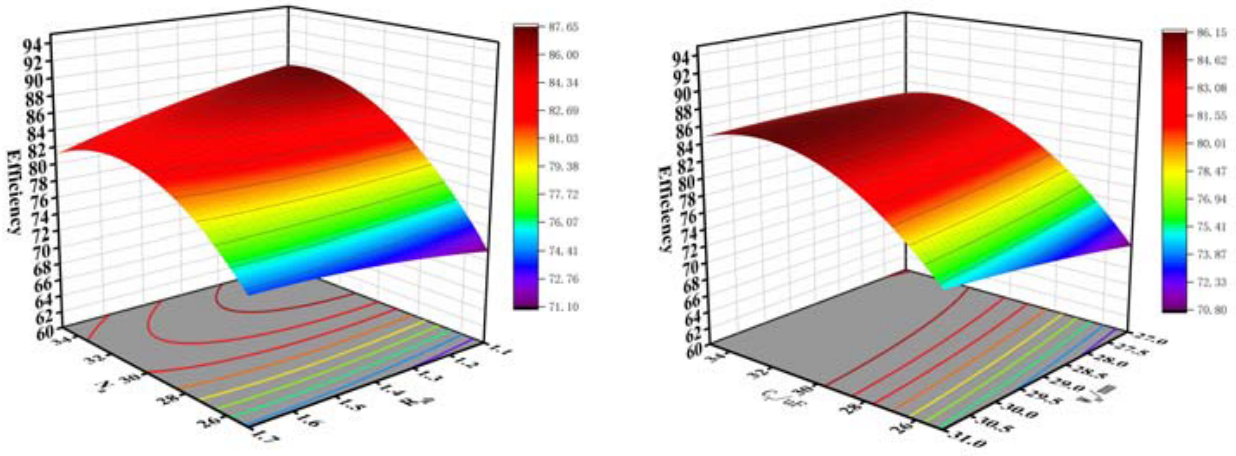

Figure 5. Efficiency interaction effect response surface.

As can be seen from Table 6, the most influential shadows on the starting torque are Na and T_m. The quadratic polynomial regression model can be used to derive the corresponding surface plot of the interaction effect of Na and T_m as variables as shown in Figure 7. From Figure 7, it can be seen that

Table 5. Analysis of variance of power factor.

Source	Squares	df	Square	P
y_2	1656.3	20	82.81	< 0.0001**
A	14.95	1	14.95	0.0017*
B	1055.76	1	1055.76	< 0.0001**
C	9.78	1	9.78	0.0079*
D	37.68	1	37.68	< 0.0001**
E	82.83	1	82.83	< 0.0001**
AB	3.01	1	3.01	0.1147
AC	0.017	1	0.017	0.9029
AD	1.6	1	1.6	0.2423
AE	0.98	1	0.98	0.3565
BC	3.02	1	3.02	0.114
BD	37.16	1	37.16	< 0.0001**
BE	23.31	1	23.31	0.0002*
CD	1.82	1	1.82	0.2134
CE	1.15	1	1.15	0.3194
DE	1.58	1	1.58	0.245
A^2	0.13	1	0.13	0.7358
B^2	99.03	1	99.03	< 0.0001**
C^2	1.6E-03	1	1.6E-03	0.9693
D^2	1.81	1	1.81	0.2144
E^2	0.67	1	0.67	0.4456
Residual	19.7	18	1.09	
Total	1676	38		

"**" indicates that the item is highly significant; "*" indicates that the item is significant

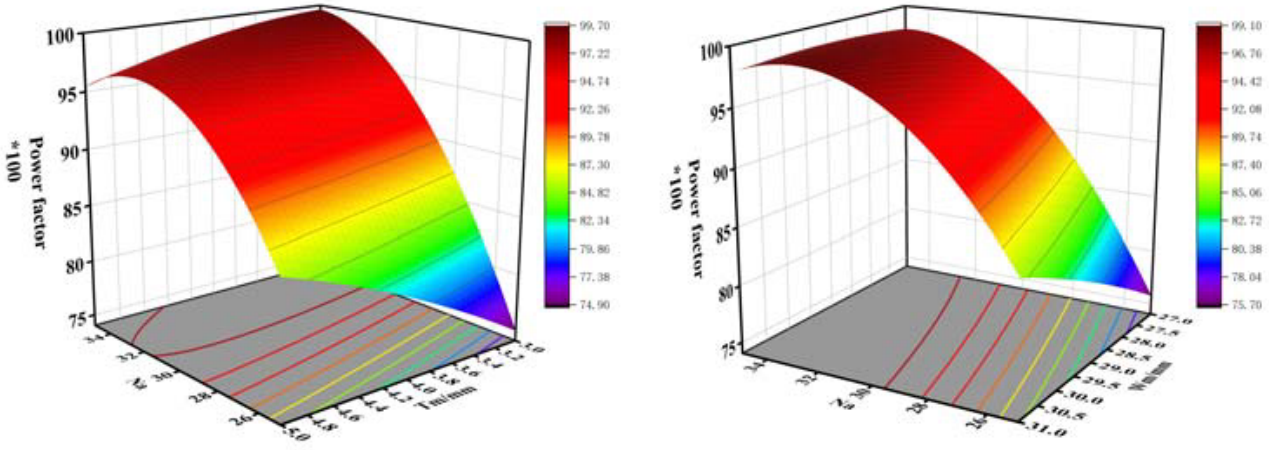

Figure 6. Power factor interaction effect response surface.

the larger T_m increases the starting torque, but when Na increases to about 28, the starting torque shows a decreasing trend. Finally, the maximum starting torque is achieved when Na is about 28 and T_m about 5.

Table 6. Analysis of variance of starting torque.

Sourse	Squares	df	Square	P
y_3	120.81	20	6.04	$< 0.0001^{**}$
A	1.37E-03	1	1.37E-03	0.9137
B	29.59	1	29.59	$< 0.0001^{**}$
C	1.16E-04	1	1.16E-04	0.9749
D	38.4	1	38.4	$< 0.0001^{**}$
E	0.13	1	0.13	0.2918
AB	0.011	1	0.011	0.7563
AC	0.028	1	0.028	0.6236
AD	1.44E-04	1	1.44E-04	0.9719
AE	2.77E-03	1	2.77E-03	0.8775
BC	20.69	1	20.69	$< 0.0001^{**}$
BD	0.18	1	0.18	0.2189
BE	0.074	1	0.074	0.4294
CD	0.04	1	0.04	0.5586
CE	0.094	1	0.094	0.3751
DE	0.31	1	0.31	0.1152
A^2	1.29E-03	1	1.29E-03	0.9162
B^2	3.66	1	3.66	$< 0.0001^{**}$
C^2	11.19	1	11.19	$< 0.0001^{**}$
D^2	0.38	1	0.38	0.083
E^2	0.014	1	0.014	0.7254
Residual	2.04	18	0.11	
Total	122.85	38		

"**" indicates that the item is highly significant; "*" indicates that the item is significant

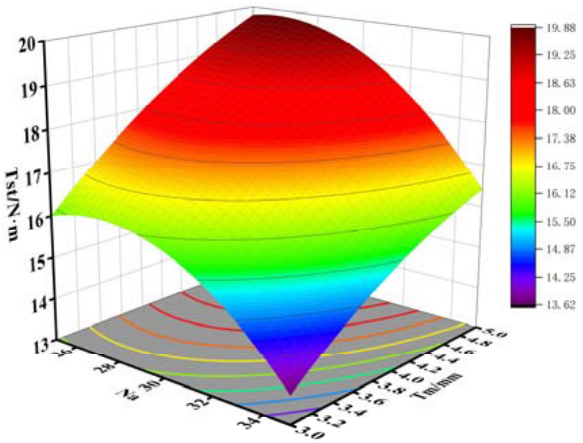

Figure 7. Strating torque interaction effect response surface.

3.4. Optimized Design and Comparative Analysis

In general, improving the efficiency of a motor is one of the important goals, as high efficiency indicates that the motor is able to convert input power to output power with less energy loss. Higher efficiency

reduces energy consumption and operating costs, is environmentally friendly, and improves the overall performance of the motor; however, power factor is also an important consideration. Power factor is the ratio between the active power consumed by the motor and the apparent power. A lower power factor can lead to increased load on the grid and affect the efficiency of power transmission and utilization. In some application scenarios, there are strict requirements for power factor. Considering that SPLSPMSM for air compressors does not require high starting torque requirements, the final efficiency, power factor, and starting torque share weights are 0.5, 0.3, and 0.2, respectively.

Through the three regression models established in the previous section, the above weights were assigned to the three optimization objectives, and by solving the regression models, the optimal parameters of A, B, C, D, and E were obtained as 25 µF, 32, 1.35, 4.8 mm, and 29.5 mm, respectively, and the above data were rounded to the standard size.

In order to verify whether the data are reliable, the data solved by the regression model are compared and analyzed with the finite element analysis (FEA) data, and the comparison results are shown in Table 7. From Table 7, it can be seen that the error between the two is very small, and the indexes are basically the same. The performance comparison between the optimized and pre-optimized motor through FEA is shown in Figure 8. From Figure 8, it can be seen that the output torque and current of the motor are improved in steady-state operation, and the starting torque of the motor is also improved when the motor is in the starting state.

Table 7. Data comparison.

Performance	Regression model	FEA	Error rate
Efficiency	85.95	85.43	0.60%
Power Factor	0.975	0.974	0.1%
Starting torque/N·m	18.512	18.446	0.3%

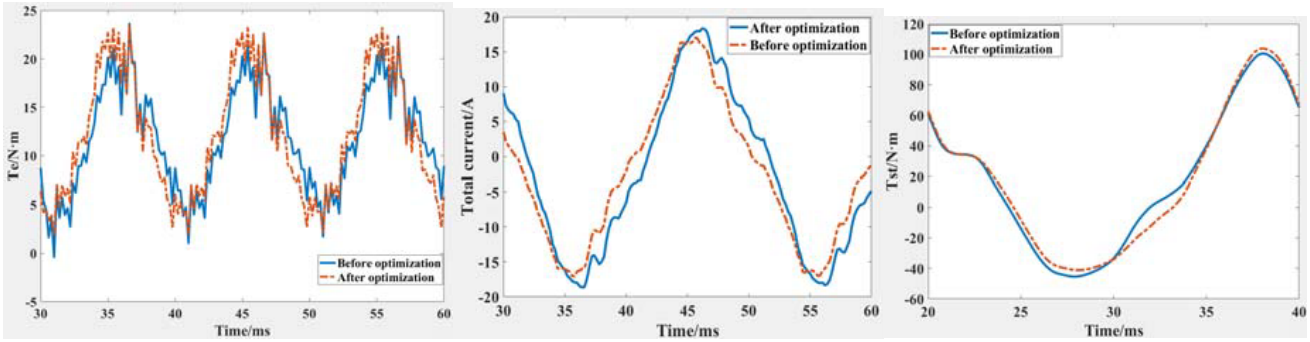

Figure 8. Performance comparison before and after optimization.

4. CONCLUSIONS

In this paper, a 1500 W SPLSPMSM is designed using the core size of an existing three-phase asynchronous motor as a reference. Since many parameters of the motor are nonlinear functions, and the parameters affect each other, the optimal value cannot be obtained by a single optimized parameter. In this paper, I propose a method to optimize the motor parameters based on the response surface method, establish a regression model with three optimization objectives, and verify the reliability of the regression model. The actual application environment of such a motor is given the corresponding weights to each optimization objective, and the motor is optimized after the preliminary design. The following conclusions were drawn in the process of optimizing the performance:

(i) In this paper, the regression models of efficiency, power factor, and starting torque are established by response surface experiments. Through experimental verification, the error rates of the regression models and the finite element analysis are only 0.6%, 0.1%, and 0.3%, which verifies that the response surface method has high reliability and accuracy in motor optimization.

(ii) In the optimization process, the improvement of rated operation performance may lead to the degradation of starting torque, and it is necessary to choose the appropriate optimization plan according to the actual environment used by such motors.

(iii) In this paper, the number of turns of stator main winding and permanent magnet size are several variables that have the most influence on the performance of SPLSPMSM in the optimized design of such motor, which provides the reference value for the subsequent optimized design.

APPENDIX A.

Number	A	B	C	D	E	y1	y2	y3
1	30	35	1.7	4	29	79.795	97.003	10.7
2	30	35	1.4	5	29	85.118	97.79	16.597
3	35	30	1.1	4	29	83.99	95.65	16.183
4	30	30	1.7	3	29	80.953	95.291	14.293
5	30	30	1.4	4	29	84.151	95.409	18.085
6	30	30	1.7	4	31	83.671	97.831	16.544
7	30	25	1.1	4	29	72.218	80.444	15.144
8	35	30	1.4	5	29	83.157	96.278	19.39
9	35	30	1.4	4	27	82.059	94.09	17.888
10	35	25	1.4	4	29	73.288	82.569	18.232
11	25	35	1.4	4	29	87.108	97.952	15.718
12	30	30	1.7	4	27	81.627	94.228	15.906
13	30	30	1.1	3	29	83.574	91.589	13.861
14	30	25	1.4	3	29	69.934	72.819	16.058
15	30	30	1.1	5	29	83.094	95.287	17.392
16	25	30	1.4	4	27	83.494	90.679	17.881
17	30	30	1.4	5	27	82.762	93.26	19.643
18	30	30	1.4	5	31	83.779	97.592	19.043
19	35	30	1.4	3	29	81.705	95.173	16.142
20	30	35	1.1	4	29	87.421	98.76	15.835
21	30	35	1.4	4	27	84.173	97.813	15.409
22	30	30	1.4	3	27	80.658	89.333	15.846
23	30	30	1.1	4	31	84.754	96.846	15.966
24	25	25	1.4	4	29	72.883	79.854	18.13
25	25	30	1.4	3	29	83.917	91.249	16.123
26	25	30	1.4	4	31	85.034	96.582	18.172
27	35	35	1.4	4	29	82.796	97.198	15.608
28	30	25	1.4	4	31	75.099	85.494	18.056
29	30	25	1.4	5	29	73.635	85.932	19.904
30	30	25	1.4	4	27	70.666	76.305	18.068
31	30	35	1.4	4	31	84.786	97.345	15.941
32	25	30	1.4	5	29	83.428	94.884	19.395
33	30	25	1.7	4	29	73.739	82.163	19.107
34	25	30	1.1	4	29	84.11	93.159	17.423
36	25	30	1.7	4	29	84.02	95.146	16.268
37	30	30	1.4	3	31	84.462	96.18	16.36
38	35	30	1.7	4	29	81.409	97.385	16.076
39	30	30	1.1	4	27	83.08	91.1	15.94

REFERENCES

1. Patil, S. S., R. T. Ugale, A. Kumar, and S. S. Revalkar, "Design of line start linear permanent magnet synchronous motor for electromagnetic catapult," *IECON 2020, The 46th Annual Conference of the IEEE Industrial Electronics Society*, 920–925, Singapore, 2020, doi: 10.1109/IECON43393.2020.9255117.
2. Dinh, B. M. and H. M. Tien, "Maximum efficiency design of line start permanent magnet synchronous motor," *2016 IEEE International Conference on Sustainable Energy Technologies (ICSET)*, 350–354, Hanoi, Vietnam, 2016, doi: 10.1109/ICSET.2016.7811808.
3. Zhao, W., M. Tian, X. Wang, and Y. Sun, "Analysis of the synchronization process and the synchronization capability for a novel 6/8-pole changing LSPMSM," *IEEE Transactions on Magnetics*, Vol. 56, No. 2, 1–6, Feb. 2020, Art no. 7507806, doi: 10.1109/TMAG.2019.2953286.
4. Lolova, I., J. Barta, G. Bramerdorfer, V. Bilek, and O. Vitek, "The optimization of single-phase line-start permanent magnet synchronous motor for household applications," *2022 International Conference on Electrical Machines (ICEM)*, 774–779, Valencia, Spain, 2022.
5. Palangar, M. F., W. L. Soong, N. Bianchi, and R.-J. Wang, "Design and optimization techniques in performance improvement of line-start permanent magnet synchronous motors: A review," *IEEE Transactions on Magnetics*, Vol. 57, No. 9, 1–14, Sept. 2021, Art no. 900214, doi: 10.1109/TMAG.2021.3098392.
6. Tian, M., X. Wang, and G. Li, "Line-start permanent magnet synchronous motor starting capability improvement using pole-changing method," *2016 IEEE 11th Conference on Industrial Electronics and Applications (ICIEA)*, 479–483, Hefei, China, 2016, doi: 10.1109/ICIEA.2016.7603631.
7. Tian, M., X. Wang, D. Wang, W. Zhao, and C. Li, "A novel line-start permanent magnet synchronous motor with 6/8 pole changing stator winding," *IEEE Transactions on Energy Conversion*, Vol. 33, No. 3, 1164–1174, Sept. 2018, doi: 10.1109/TEC.2018.2826550.
8. Zhao, Y., D. Li, M. Lin, and R. Qu, "Investigation of line-start permanent magnet vernier machine with different rotor topologies," *IEEE Journal of Emerging and Selected Topics in Power Electronics*, Vol. 10, No. 3, 2859–2870, June 2022, doi: 10.1109/JESTPE.2021.3061120.
9. Yan, B., Y. Yang, and X. Wang, "Design of a large capacity line-start permanent magnet synchronous motor equipped with hybrid salient rotor," *IEEE Transactions on Industrial Electronics*, Vol. 68, No. 8, 6662–6671, Aug. 2021, doi: 10.1109/TIE.2020.3008360.
10. Ghoroghchian, F., A. D. Aliabad, and E. Amiri, "Dual-pole line start permanent magnet synchronous motor with series-parallel magnetic structure," *IEEE Transactions on Energy Conversion*, Vol. 35, No. 2, 854–862, Jun. 2020, doi: 10.1109/TEC.2020.2967241.
11. Tian, M., X. Wang, W. Zhao, and C. Li, "Analysis on the starting and synchronization capabilities for a novel 6/8 pole changing line-start permanent magnet synchronous motor," *2018 IEEE International Magnetics Conference (INTERMAG)*, 1–2, Singapore, 2018, doi: 10.1109/INTMAG.2018.8508868.
12. Lyskawinski, W., C. Jedryczka, and W. Szelag, "Influence of magnet and cage shape on properties of the line start synchronous motor with powder hybrid rotor," *2017 International Symposium on Electrical Machines (SME)*, 1–6, Naleczow, Poland, 2017, doi: 10.1109/ISEM.2017.7993556.
13. Maraaba, L. S., A. S. Milhem, I. A. Nemer, H. Al-Duwaish, and M. A. Abido, "Convolutional neural network-based inter-turn fault diagnosis in LSPMSMs," *IEEE Access*, Vol. 8, 81960–81970, 2020, doi: 10.1109/ACCESS.2020.2991137.
14. Maraaba, L. S., Z. M. Al-Hamouz, and M. A. Abido, "An accurate tool for detecting stator inter-turn fault in LSPMSM," *IEEE Access*, Vol. 7, 88622–88634, 2019, doi: 10.1109/ACCESS.2019.2923812.
15. Dogan, Z. and K. Tetik, "Diagnosis of inter-turn faults based on fault harmonic component tracking in LSPMSMs working under nonstationary conditions," *IEEE Access*, Vol. 9, 92101–92112, 2021, doi: 10.1109/ACCESS.2021.3092605.

16. Palangar, M. F., W. L. Soong, and A. Mahmoudi, "Outer and inner rotor line-start permanent-magnet synchronous motors: An electromagnetic and thermal comparison study," *2021 IEEE Energy Conversion Congress and Exposition (ECCE)*, 4226–4233, Vancouver, BC, Canada, 2021, doi: 10.1109/ECCE47101.2021.9595574.
17. Palangar, M. F., A. Mahmoudi, S. Kahourzade, and W. L. Soong, "Electromagnetic and thermal analysis of a line-start permanent-magnet synchronous motor," *2020 IEEE Energy Conversion Congress and Exposition (ECCE)*, 502–508, Detroit, MI, USA, 2020, doi: 10.1109/ECCE44975.2020.9235632.
18. Gnaciński, P., A. Muc, and M. Pepliński, "Influence of voltage subharmonics on line start permanent magnet synchronous motor," *IEEE Access*, Vol. 9, 164275–164281, 2021, doi: 10.1109/ACCESS.2021.3133279.
19. Zhang, S., B. Cui, J. Li, Y. Shi, N. Pan, and Y. Han, "Research on torque pulsation suppression of permanent magnet synchronous motor based on harmonic injection," *2023 IEEE International Conference on Control, Electronics and Computer Technology (ICCECT)*, 1142–1146, Jilin, China, 2023, doi: 10.1109/ICCECT57938.2023.10141219.
20. Xie, S., X. Feng, P. Gu, W. Zhang, Z. Lei, and C. Zhao, "Harmonic suppression of open-winding pmsm system with common DC bus based on improved PIR control," *2023 International Conference on Power Energy Systems and Applications (ICoPESA)*, 777–784, Nanjing, China, 2023, doi: 10.1109/ICoPESA56898.2023.10141410.
21. Shang, J., W. Tang, and C. Liu, "Optimization of electromagnetic performance of single phase line-start permanent magnet synchronous motor based on the finite element method," *2019 22nd International Conference on Electrical Machines and Systems (ICEMS)*, 1–6, Harbin, China, 2019, doi: 10.1109/ICEMS.2019.8922439.